Improvements in the representation of the Indian summer monsoon in the NCEP climate forecast system version 2

Rodrigo J. Bombardi, Edwin K. Schneider, Lawrence Marx, Subhadeep Halder, Bohar Singh, Ahmed B. Tawfik, Paul A. Dirmeyer, et al

Climate Dynamics
Observational, Theoretical and Computational Research on the Climate System

ISSN 0930-7575

Clim Dyn
DOI 10.1007/s00382-015-2484-6

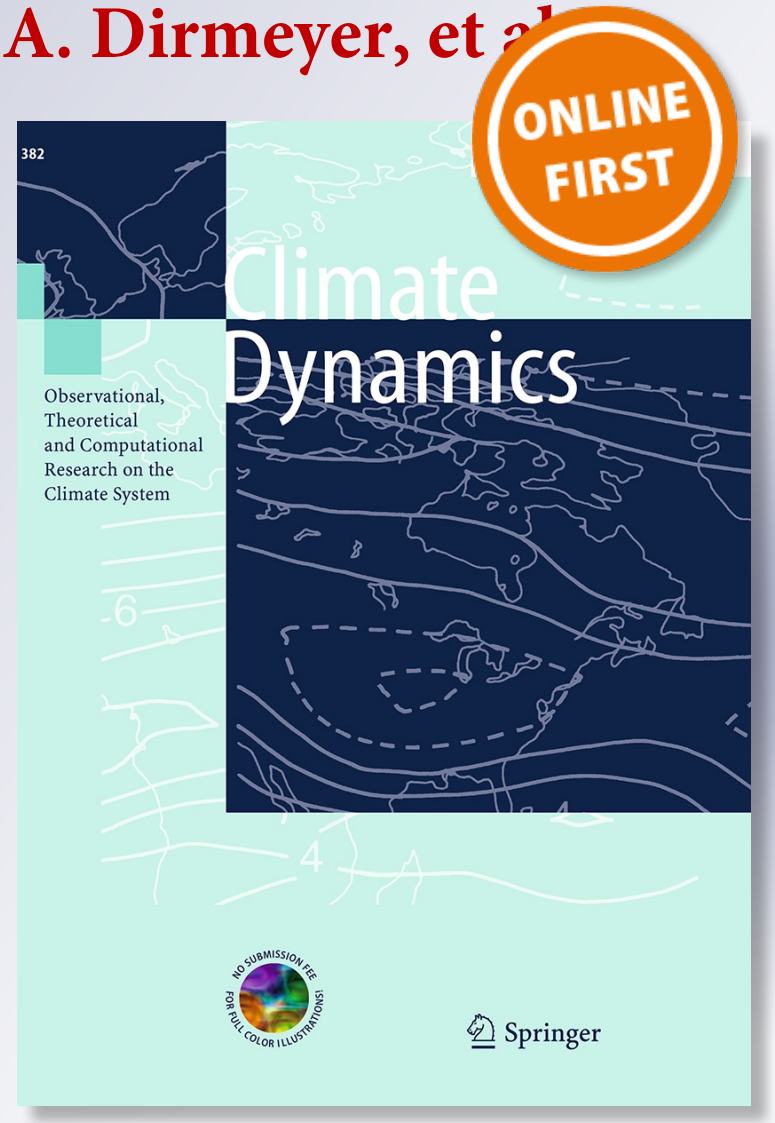

Springer

Your article is protected by copyright and all rights are held exclusively by Springer-Verlag Berlin Heidelberg. This e-offprint is for personal use only and shall not be self-archived in electronic repositories. If you wish to self-archive your article, please use the accepted manuscript version for posting on your own website. You may further deposit the accepted manuscript version in any repository, provided it is only made publicly available 12 months after official publication or later and provided acknowledgement is given to the original source of publication and a link is inserted to the published article on Springer's website. The link must be accompanied by the following text: "The final publication is available at link.springer.com".

Author's personal copy

Clim Dyn
DOI 10.1007/s00382-015-2484-6

Improvements in the representation of the Indian summer monsoon in the NCEP climate forecast system version 2

Rodrigo J. Bombardi · Edwin K. Schneider · Lawrence Marx · Subhadeep Halder · Bohar Singh · Ahmed B. Tawfik · Paul A. Dirmeyer · James L. Kinter III

Received: 6 August 2014 / Accepted: 12 January 2015
© Springer-Verlag Berlin Heidelberg 2015

Abstract A new triggering mechanism for deep convection based on the heated condensation framework (HCF) is implemented into the National Centers for Environmental Prediction climate forecast system version 2 (CFSv2). The new trigger is added as an additional criterion in the simplified Arakawa–Schubert scheme for deep convection. Seasonal forecasts are performed to evaluate the influence of the new triggering mechanism in the representation of the Indian summer monsoon in the CFSv2. The HCF trigger improves the seasonal representation of precipitation over the Indian subcontinent. The new triggering mechanism leads to a significant, albeit relatively small, improvement in the bias of seasonal precipitation totals. In addition, the new trigger improves the representation of the seasonal precipitation cycle including the monsoon onset, and the probability distribution of precipitation intensities. The mechanism whereby the HCF improves convection over India seems to be related not only to a better representation of the background state of atmospheric convection but also to an increase in the frequency in which SAS is triggered. As a result, there was an increase in convective precipitation over India favored by the availability of moist convective instability. The increase in precipitation intensity leads to a reduction in the dry bias.

R. J. Bombardi (✉) · E. K. Schneider · S. Halder · B. Singh · A. B. Tawfik · P. A. Dirmeyer · J. L. Kinter III
Department of Atmospheric, Oceanic, and Earth Sciences, College of Science, George Mason University, 4400 University Drive, Fairfax, VA 22033, USA
e-mail: rbombard@gmu.edu

E. K. Schneider · L. Marx · A. B. Tawfik · P. A. Dirmeyer · J. L. Kinter III
Center for Ocean–Land–Atmosphere Studies, Institute of Global Environment and Society, Calverton, MA, USA

Keywords Trigger function · CFSv2 · Indian summer monsoon · Seasonal predictability · Convection

1 Introduction

As an operational forecast model, the National Centers for Environmental Prediction (NCEP) atmosphere–ocean global coupled model (AOGCM), the climate forecast system, is under continuous development. The previous version of the prediction system (CFSv1; Saha et al. 2006) was found to be among the best models to represent the Indian summer monsoon rainfall (Pokhrel et al. 2012). In addition, the CFSv1 was able to represent major patterns of precipitation and circulation associated with the Asian monsoon. On the other hand, the model showed a strong negative bias in precipitation over central India (Yang et al. 2008). The development of the climate forecast system version 2 (CFSv2; Saha et al. 2014a) resulted in many improvements, such as a better representation of the pressure gradient between the southern Indian Ocean and the northern Indian subcontinent (Saha et al. 2014b). However, the negative precipitation bias still persists over central India (Zhu and Shukla 2013; Silva et al. 2014; Saha et al. 2014b).

This work focuses on the reduction of the CFSv2 precipitation bias over central India. Our approach is based on the hypothesis that the triggering mechanism for deep convection currently in use in the CFSv2 could be modified to represent tropical convection conditions more appropriately. A convective triggering function is a criterion or a set of criteria that have to be satisfied in order for the initiation of convection to occur (e.g. Chao 2013). However, the initiation of convection refers only to the starting of an event and it is different from the continuation of convection (Chao 2013). But the common usage of this term in the

Published online: 23 January 2015

Author's personal copy

cumulus parameterization research has distorted this meaning to include the continuation of convection. There are a variety of convective trigger functions in use in current atmospheric models. Recently, Suhas and Zhang (2014) performed a comprehensive evaluation of the main trigger functions currently in use in global and regional atmospheric models and provided some suggestion for optimization of those trigger functions. The authors verified that many of the trigger functions show poor skill in activating convection at the right time and location.

In addition, according to Tawfik and Dirmeyer (2014), conventional methods for triggering deep convection neglect the incremental growth of the planetary boundary layer (PBL). Most are based on metrics dependent on atmospheric states at arbitrary heights, or they are based on lifting a parcel from a certain height without allowing the parcel to mix with its surroundings. As a consequence, these methods present limitations related to the characterization of the atmospheric state in relation to convection.

Therefore, Tawfik and Dirmeyer (2014) developed a new triggering mechanism for convection, named heated condensation framework (HCF), based on a diagnostic analysis of land-surface controls of boundary layer properties and cloud formation. The HCF was envisioned as an alternative diagnostic to represent the atmospheric background state with respect to convection. This method introduces the concepts of buoyant condensation level (BCL) and buoyant mixing temperature (θ_{BM}), which can be defined from standard profiles of temperature and specific humidity. These two variables quantify how conditioned the atmosphere is to moist free convection due to surface heating, which is characterized by the near surface potential temperature (θ_{2m}). Rather than lifting a hypothetical unmixed parcel, the HCF constructs a hypothetical boundary layer by incrementally inputting heat at the surface.

The HCF takes into account both large-scale (as the atmosphere background state represented by θ_{BM}) and local surface heating (as represented by θ_{2m}) conditions for convection. Therefore, the HCF trigger requires the atmosphere to be sufficiently pre-conditioned to convection with sufficient local heating in order to initiate convection. In summary, θ_{BM} is a measurement of the θ_{2m} that is required in order for the PBL to attain the BCL height. The lower the θ_{BM} the more preconditioned the atmosphere is to moist convection (Tawfik and Dirmeyer 2014). On the other hand, the original trigger criterion in the CFSv2 merely requires that the pressure difference between the lifting condensation level and maximum moist static energy (usually the

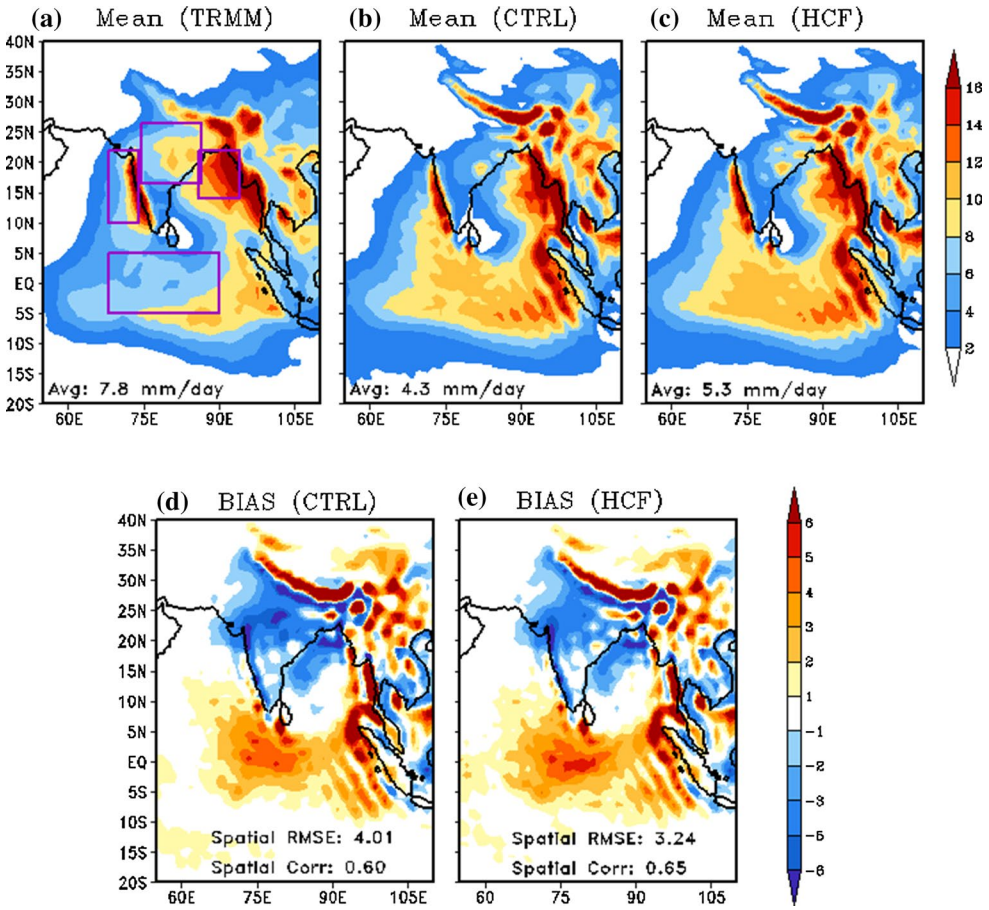

Fig. 1 Mean JJAS precipitation (mm/day) for **a** TRMM, **b** CTRL, and **c** HCF and JJAS precipitation bias for **d** CTRL and **e** HCF. **a** Shows some regions of interest defined as Central India (74.5°E–86.5°E, 16.5°N–26.5°N), the equatorial Indian Ocean (68°E–90°E, 5°S–5°N), the Arabian Sea (68°E–74°E, 10°N–22°N), and the Bay of Bengal (86°E–94°E, 14°N–22°N). The figure also shows information about precipitation average, spatial RMSE, and spatial correlation (in relation to TRMM) for the central India region

Author's personal copy

first layer of the atmosphere) to be less than an arbitrary threshold (Han and Pan 2011; Suhas and Zhang 2014). Hence, the current trigger function in the CFSv2 may be lacking a physical treatment of convective initiation and the HCF is a physical approach to triggering convection.

This work evaluates the impact of implementing the HCF trigger into the CFSv2 in seasonal ensemble simulations. This study is part of the National Monsoon Mission project supported by the Ministry of Earth Sciences, Government of India. The project has the objective of improving the seasonal forecast for the Indian Monsoon. Section 2 describes the CFSv2 and the numerical experiments. The impact of HCF on seasonal simulations is shown in Sect. 3. Section 4 shows the impact of the new triggering mechanism on daily precipitation and on the monsoon timing. The representation of the diurnal cycle of precipitation by the CFSv2 is evaluated in Sect. 5. Possible mechanisms are explored in Sect. 6. The conclusions are presented in Sect. 6.

2 Model and experiments

2.1 Model

The atmospheric component of the CFSv2 AOGCM is based on the NCEP global forecast system (GFS) model. Simulations were performed with spectral discretization at T126 resolution (about 100 km grid spacing) and 64 levels in the vertical. The ocean component of the CFSv2 is the Modular Ocean Model version 4 (MOM4) (Griffies et al. 2004). The ocean model was configured with 1/2° horizontal resolution, increasing to 1/4° meridional resolution in the deep tropics, and 40 vertical levels.

The HCF trigger was implemented into the simplified Arakawa–Schubert (SAS) scheme for deep convection (Pan and Wu 1995; Hong and Pan 1998) in the CFSv2. SAS is a mass-flux column model organized as follows: First, the starting point of convection is defined as the vertical level with the maximum moist static energy. The starting point is assumed to be below 700 hPa. Next, the cloud base is defined as the level of free convection (LFC), which is detected based on the atmospheric stability above the starting point (maximum moist static energy). There are two SAS routines currently in use in the CFSv2, commonly known as old SAS and new SAS. The current triggering mechanism in use in the SAS scheme in the CFSv2 is based on the vertical distance between the starting point and the LFC. If the difference between these two levels is less than 150 hPa in the old SAS scheme (or between 120 and 180 hPa in the new SAS scheme), convection is allowed to occur (Han and Pan 2011; Suhas and Zhang 2014). The triggering mechanism is a necessary but not sufficient condition for deep convection in the SAS scheme; many other factors such as entrainment, detrainment, and cloud work also play a role in the development of convection. A detailed description of the SAS scheme can be found in Pan and Wu (1995), Hong and Pan (1998), and Han and Pan (2011).

The HCF convective trigger scheme was implemented into the CFSv2 as an alternative criterion for convection to occur, where convection is initiated when the PBL intersects the BCL. That is, the SAS scheme will initiate if either the old or the new trigger criterion are met. Tests show that, at this point, this is the best configuration for the initiation of deep convection in the SAS scheme. Other configurations such as including HCF as an additional criterion for convection or completely replacing the original criterion by the HCF trigger resulted in substantially less convective precipitation over the whole tropics (not shown). The results presented here were based on the old SAS routine.

2.2 Experiments

We performed 7-month long ensemble retrospective predictions with (denoted HCF) and without (CTRL) the HCF trigger mechanism. Four ensemble members were generated for each year from 1998 to 2010 starting in the first 4 days of April. Due to storage issues, we could only retain daily averages in our seasonal simulations. Therefore, in order to evaluate the diurnal cycle of precipitation we performed two other sets of short simulations of approximately

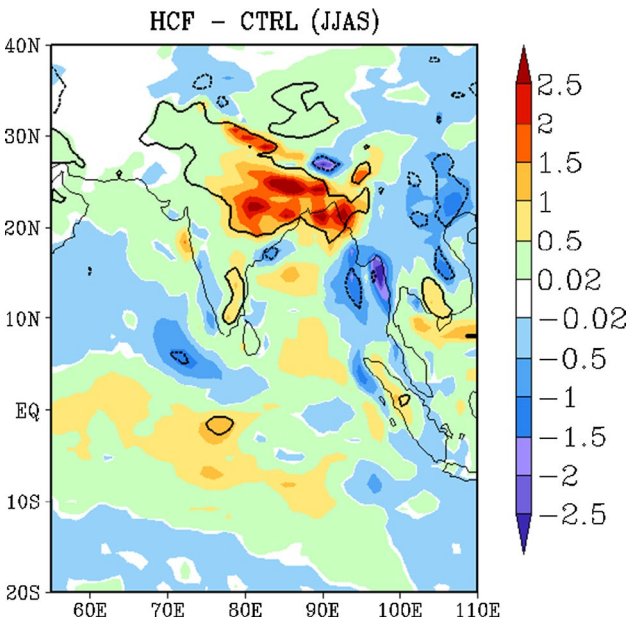

Fig. 2 Mean JJAS precipitation (mm/day) difference between HCF and CTRL experiments. The contour indicates regions where the difference is statistically significant at 5 % level according to a *t* test

Author's personal copy

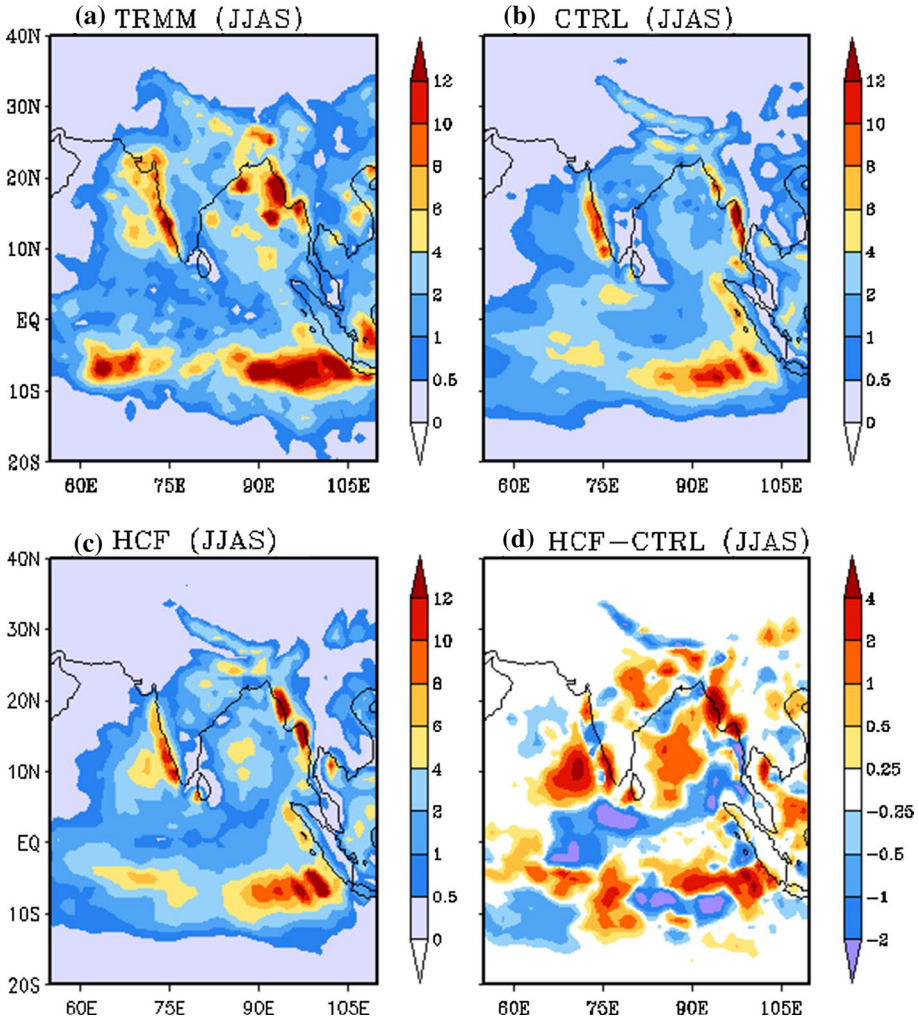

Fig. 3 Mean standard deviation of JJAS precipitation (mm/day) for **a** TRMM, **b** CTRL, **c** HCF and **d** mean standard deviation difference between HCF and CTRL

2 weeks. We used the same configurations as the seasonal simulations but these short simulations were initialized in the peak of the monsoon season starting in mid July (July 14, 15, 16, and 17). The initial conditions are from the NCEP climate forecast system reanalysis (CFSR; Saha et al. 2010). The implementation of the HCF trigger did not increase the CFSv2 integration time. Simulation results are compared to the TRMM precipitation analysis (Huffman et al. 2007), to the ERA-interim reanalysis (Dee et al. 2011) and to the Modern Era-Retrospective Analysis For Research and Applications (MERRA) reanalysis (Rienecker et al. 2011).

3 Seasonal variability

Figure 1 presents the observed mean precipitation between June and September (JJAS) for the TRMM dataset and both CTRL and HCF experiments. In addition, some regions of interest for this work are shown in Fig. 1a defined as Central India (74.5°E–86.5°E, 16.5°N–26.5°N), the equatorial Indian Ocean (68°E–90°E, 5°S–5°N), the Arabian Sea (68°E–74°E, 10°N–22°N), and the Bay of Bengal (86°E–94°E, 14°N–22°N). The CFSv2 represents the main spatial pattern of JJAS precipitation, with maxima over the west coast of India and the west coast of Southeast Asia. However, the model underestimates the precipitation over India and overestimates the precipitation over the equatorial Indian Ocean (Fig. 1). We verify a small improvement in the seasonal precipitation over the Indian subcontinent in the HCF experiment in comparison to the CTRL experiment (Fig. 1d, e). The HCF trigger mechanism increases the JJAS precipitation over south, central, and northeast India. Although the improvement is small in comparison to the overall precipitation bias, it is a significant improvement of up to 2.5 mm/day (Fig. 2).

A well-known problem in general circulation models and meso-scale models is the generation of excessive precipitation over steep and high mountains. The CFSv2 is not an exception (Fig. 1). The implementation of the HCF trigger does not show any clear improvement of this problem (Figs. 1, 2). Chao (2012) verified that the main cause of

Author's personal copy

this problem is the model's inability to transport heat out of the boundary layer due to ventilation processes that happen on the subgrid-scale slopes of regions with steep and high mountains. A parameterization scheme was developed to simulate the ventilation process and tests with the NASA Goddard Earth Observing System GCM version 5 have shown good results (Chao 2012).

The new trigger also improves the magnitude of the precipitation variability, defined by the standard deviation, over both land and ocean (Fig. 3). The HCF experiment shows increased precipitation variability over central India, over the Arabian Sea near to the west coast of India, over the Bay of Bengal, and over the western equatorial Indian Ocean (Fig. 3c, d). In addition, the new trigger appropriately decreases the precipitation variability over the ocean adjacent to the southernmost part of India (Fig. 3b–d).

To explore the impact of the new trigger on circulation, changes in the 850 and 200 hPa winds are examined. Figure 4 shows the biases of low and high level winds in both CTRL and HCF simulations in relation to ERA-interim. We verify a small reduction in the magnitude of the 850 hPa zonal wind bias over northeastern India along the Himalayas as well as a reduction in the equatorial India Ocean (Fig. 4a, b). The magnitude of the 850 hPa meridional wind bias shows only slight differences, with increased magnitudes over the western coast of India (Fig. 4c, d). There is a noticeable reduction in the magnitude of the 200 hPa zonal wind bias over the Arabian Sea, India, and the equatorial Indian Ocean (Fig. 4e, f) as well as in the meridional wind over India (Fig. 4g, h). In summary, the new trigger mechanism reduced the low level wind along the Himalayas and reduced the intensity of the upper level winds over central India (significant at 95 % confidence level) during JJAS, resulting in slightly more realistic large-scale wind circulation over India.

4 Daily precipitation variability and monsoon timing

Figure 5 shows the distribution of daily precipitation over Central India for TRMM and both CTRL and HCF experiments. The CFSv2 overestimates low intensity precipitation (<4 mm/day) and underestimates high intensity precipitation (>6 mm/day), which is a common bias in convective parameterization schemes (e.g. Kang et al. 2014). The HCF shows a decrease in low intensity precipitation and an increase in high intensity precipitation in comparison to CTRL (Fig. 5), characterizing a small improvement for both low and high intensity precipitation. The HCF and CTRL distributions are different from each other at 95 % confidence level according to a maximum likelihood ratio test.

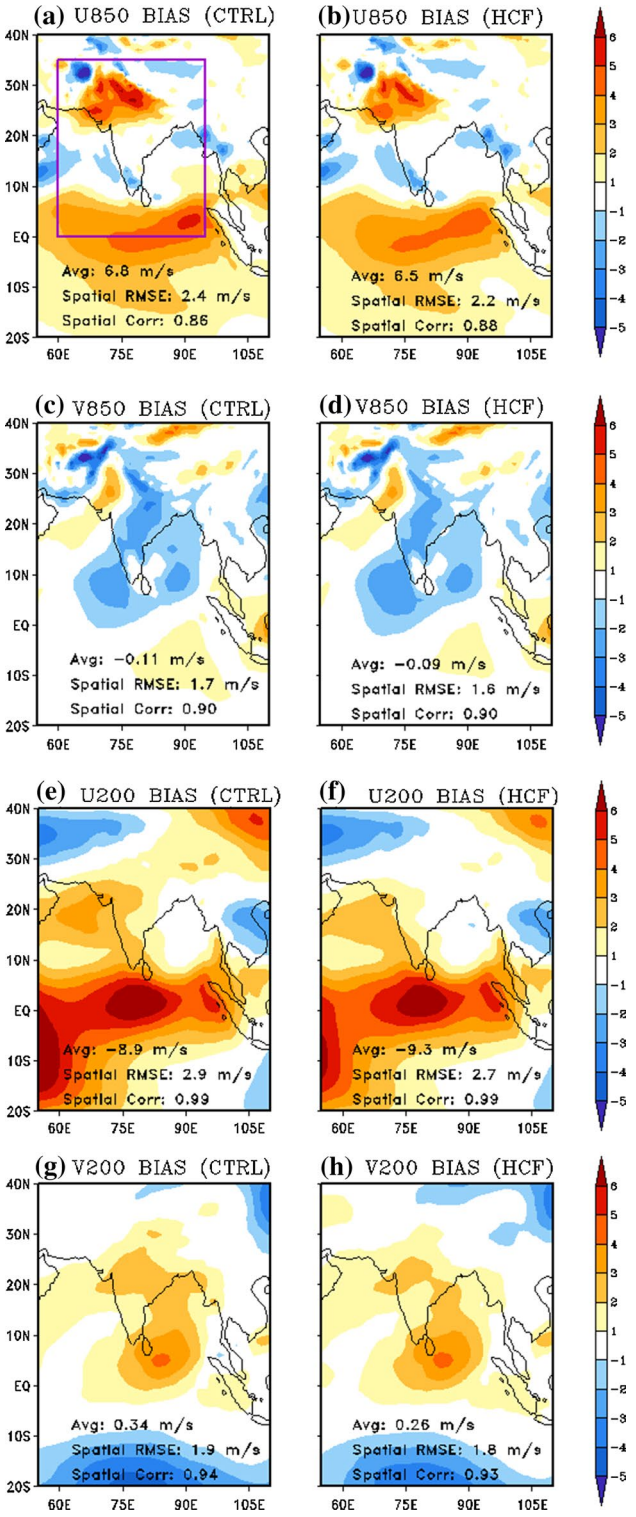

Fig. 4 CTRL (*left*) and HCF (*right*) mean JJAS wind bias (m/s) in comparison to ERA-Interim. The panel are: **a**, **b** zonal wind at 850 hPa, **c**, **d** meridional wind at 850 hPa, **e**, **f** zonal wind at 200 hPa, and **g**, **h** meridional wind at 200 hPa. The figure also shows information about wind average, spatial RMSE, and spatial correlation (in relation to ERA-Interim) for the domain shown in **a**

Author's personal copy

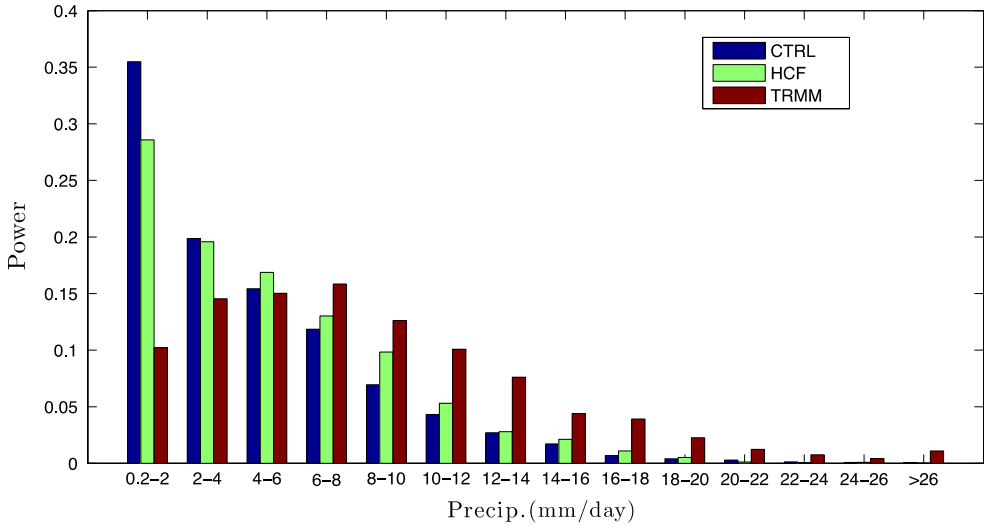

Fig. 5 Frequency distribution of daily precipitation (mm/day) for TRMM, HCF, and CTRL over Central India (16.5°N–26.5°N, 74.5°E–86.5°E). The HCF and CTRL distributions are different at 95 % confidence level according to a maximum likelihood ratio test

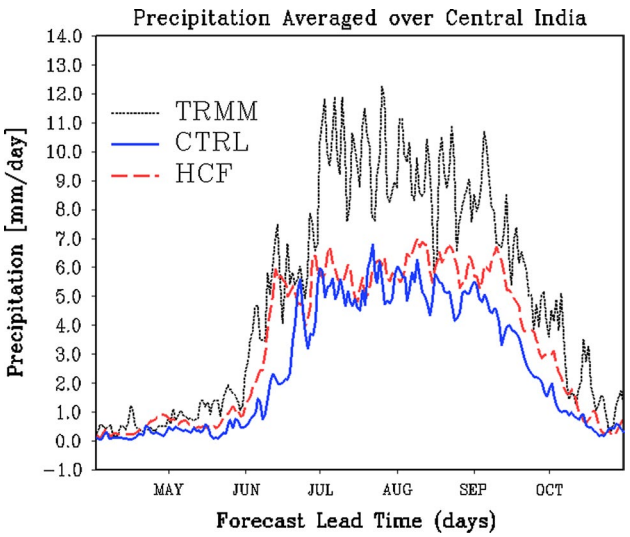

Fig. 6 Mean seasonal cycle of precipitation (mm/day) for the TRMM and for both CTRL and HCF simulations, spatially averaged over Central India (16.5°N–26.5°N, 74.5°E–86.5°E)

These results suggest that the HCF simulations are characterized by stronger convective activity than the CTRL. Considering that the HCF trigger was implemented as an alternative condition for convection to initiate, one of the modifications introduced by the HCF trigger is an increase in the frequency in which SAS is activated. Since the model time step is of about 10 min, at every 10 min there is a probability that SAS will generate precipitation. The inclusion of the HCF criterion as an alternative condition increased that probability. The mechanisms will be further investigated in Sect. 6.

There is also a clear improvement in the seasonal cycle of the precipitation over central India in the HCF experiment in comparison to the CTRL experiment (Fig. 6). Although the CFSv2 still strongly underestimates the maximum monsoonal rainfall during July and August, the new trigger improves the representation of the onset and withdrawal dates of the Indian rainy season (Fig. 6).

To evaluate the CFSv2 representation of the monsoon timing we applied a method created by Liebmann and Marengo (2001) and adapted by Bombardi and Carvalho (2009) to define the onset and the demise of the rainy season. This method was applied to the TRMM dataset and to each member of the CFSv2 experiments separately. The method depends only on precipitation and it is based on Eq. 1, where S is the accumulated precipitation anomaly, R is the daily precipitation, and Rm is the annual climatological mean.

$$S = \sum_{t=1} (R(t) - Rm) \tag{1}$$

The accumulated precipitation anomalies are computed for each grid point starting from the dry season. Initially S has negative values. Once the precipitation becomes frequent, the S curve presents an inflection and starts to increase. The S curve is smoothed by a 1-2-1 filter and the first derivative of the smoothed curve is calculated. The date when the signal of the first derivative of the smoothed S changes from negative to positive is taken as the onset of the rainy season. Analogously, by starting the calculation of the accumulated precipitation anomalies in the wet season, the date when the derivative of S changes from positive to negative is taken as the withdrawal of the rainy season.

Figure 7a shows the progression of the onset of the Indian monsoon in day-of-year (DOY) in the TRMM

Author's personal copy

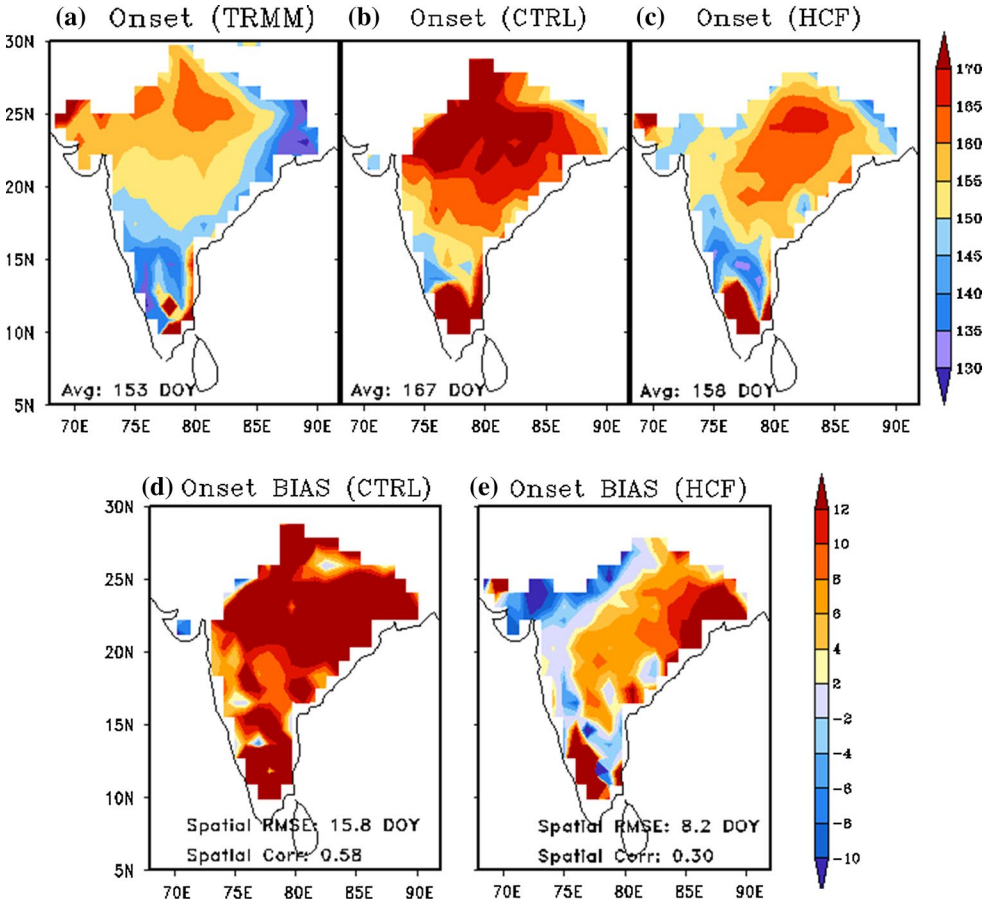

Fig. 7 Mean onset date of the Indian summer monsoon (day of year) for **a** TRMM, **b** CTRL, and **c** HCF. Onset date bias for **d** CTRL and **e** HCF. The figure also shows information about onset date average, spatial RMSE, and spatial correlation (in relation to TRMM) for the central India region

dataset. We observe a northwestward propagation of the monsoon starting in late May (DOY 140) in the south, to early June (DOY 155) over central India, and up to mid July (DOY 165) over northwestern India. These results are consistent with the climatological northwestward progression of the Indian Monsoon (e.g. Joseph et al. 1994; Fasullo and Webster 2002). The CFSv2 does not seem to realistically reproduce the northwestward propagation of the monsoon (Fig. 7b, c), a problem also present in CFSv1 (Yang et al. 2008). The northwestward propagation of the monsoon seems to be even less realistic in the HCF experiments than in the CTRL experiments (Fig. 7b–e). However, the HCF experiments show monsoon onset dates closer to the observed values in comparison to the CTRL experiment, especially over central India (Fig. 7b–e).

5 Diurnal cycle of precipitation

Figure 8 shows the diurnal cycle of precipitation from TRMM and from the CTRL and HCF short simulations. The figure also shows the partitioning between convective and large-scale simulated precipitation. There are only small differences in the diurnal cycle of precipitation simulated by HCF in comparison to CTRL (Fig. 8). Over central India (Fig. 8a), CFSv2 overestimates precipitation from 0Z to 9Z and underestimates the precipitation from 12Z to 21Z. CFSv2 highly overestimates precipitation over the Equatorial Indian Ocean (Fig. 8b) and over the Arabian Sea (Fig. 8c) but it represents well the diurnal cycle of precipitation over the Bay of Bengal (Fig. 8d). We are currently testing a new version of the HCF trigger with a better representation of initialization of convection over the ocean that includes buoyancy adjustment due to moisture that are known to be especially important in the tropics (Stevens 2005; Smith et al. 2012).

In addition, there was no clear improvement in short-range forecast skill (first 2 weeks) considering the domains of North America, India, NINO3.4, the tropics, the Northern Hemisphere, and the Southern Hemisphere (not shown). The forecast skill was evaluated by the lagged anomaly correlation of geopotential height at 500 hPa.

6 Mechanisms

To explore the possible mechanisms whereby the HCF trigger improves precipitation over India, we analyze its impact

Author's personal copy

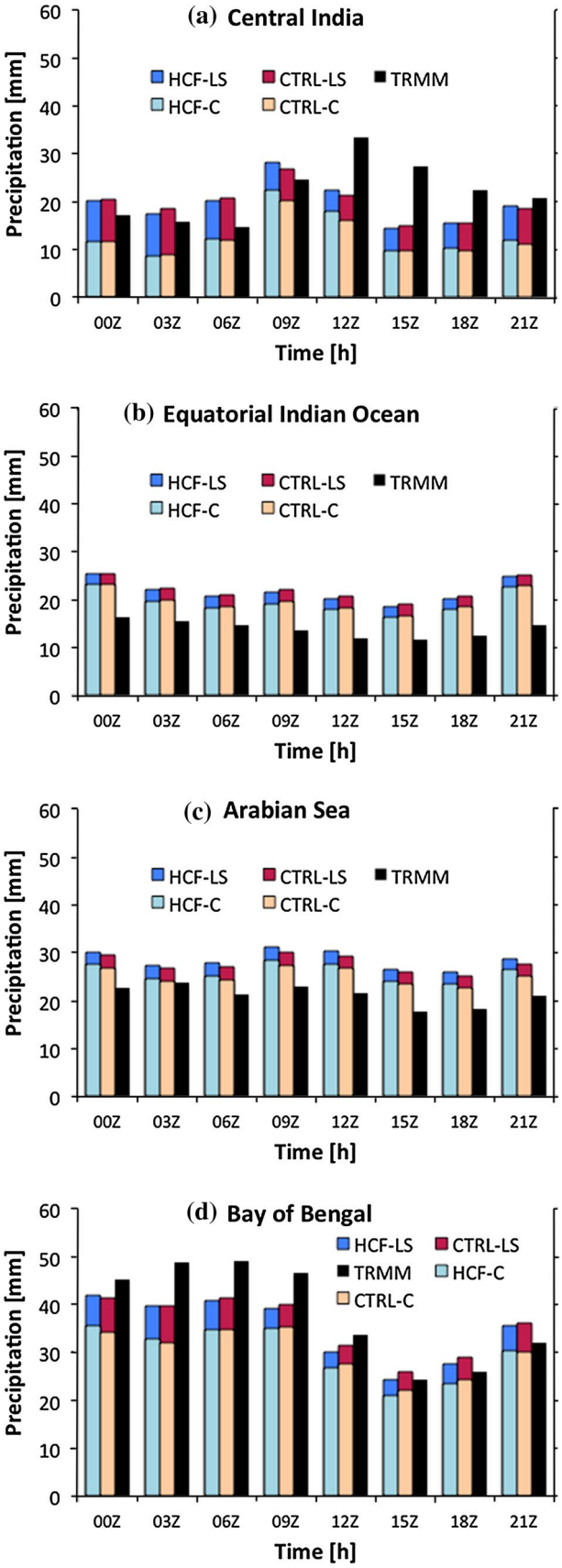

Fig. 8 Diurnal cycle of precipitation from TRMM and short simulations starting in mid July. Spatially averaged over **a** Central India (74.5°E–86.5°E, 16.5°N–26.5°N), **b** the equatorial Indian Ocean (68°E–90°E, 5°S–5°N), **c** the Arabian Sea (68°E–74°E, 10°N–22°N), and **d** the Bay of Bengal (86°E–94°E, 14°N–22°N). The figure also shows the partitioning between simulated large-scale (LS) and convective (C) precipitation

in the surface radiative balance (Figs. 9, 10, 11), cloud condensate (Fig. 12), and convective instability (Fig. 13). The CFSv2 overestimates the net surface shortwave radiation over most of our region of interest, especially over Myanmar and the Himalayans (Fig. 9). The net surface shortwave radiation bias over central India is slightly larger (in magnitude) in the HCF than in the CTRL simulations (Fig. 9d, e). On the other hand, the CFSv2 underestimates net surface longwave radiation over most of our region of interest (Fig. 10). In addition, the net surface longwave radiation bias is slightly smaller (in magnitude) in the HCF than in the CTRL hindcasts (Fig. 10d, e).**Fig. 10** As Fig. 9 for net surface longwave radiation

Simulations with the new triggering mechanisms show increased net surface shortwave radiation over central and southern India as well as increased net surface longwave radiation over central and northern India (Fig. 11). Thus, the surface is receiving more shortwave radiation (Fig. 11a) and losing less longwave radiation (Fig. 11b) to the atmosphere in the HCF than in the CTRL simulations.

Figure 12 shows profiles of total cloud condensate (Cloud water and ice) as an estimate of cloud cover for both simulations and for the MERRA reanalysis over Central India (Fig. 12a), the equatorial Indian Ocean (Fig. 12c), the Arabian Sea (Fig. 12e), and the Bay of Bengal (Fig. 12h). We chose to compare CFSv2 with MERRA due to the good representation of water and energy cycles in MERRA (Rienecker et al. 2012) related to the assimilation of cloud condensate and cloud fraction (Rienecker et al. 2008). Observational analyses by Kumar et al. (2013) showed that shallow clouds are more prevalent over the Western Ghats region whereas deep clouds (particularly in the mid and upper troposphere) are more prevalent along the Myanmar coast, which is consistent with the cloud condensate profiles from MERRA (Fig. 12e, h).

The CFSv2 underestimates the amount of high clouds over all four regions (Fig. 12) as well as the amount of low clouds over the Arabian Sea (Fig. 12e) and over the equatorial Indian Ocean (Fig. 12g). In addition, the middle clouds in the CFSv2 are located lower in the troposphere in comparison to MERRA (Fig. 12). Over central India, the main effect of the HCF trigger is to remove cloud water from the middle troposphere and to increase it in the higher troposphere (Fig. 12b). To a lesser degree, similar effects are

Author's personal copy

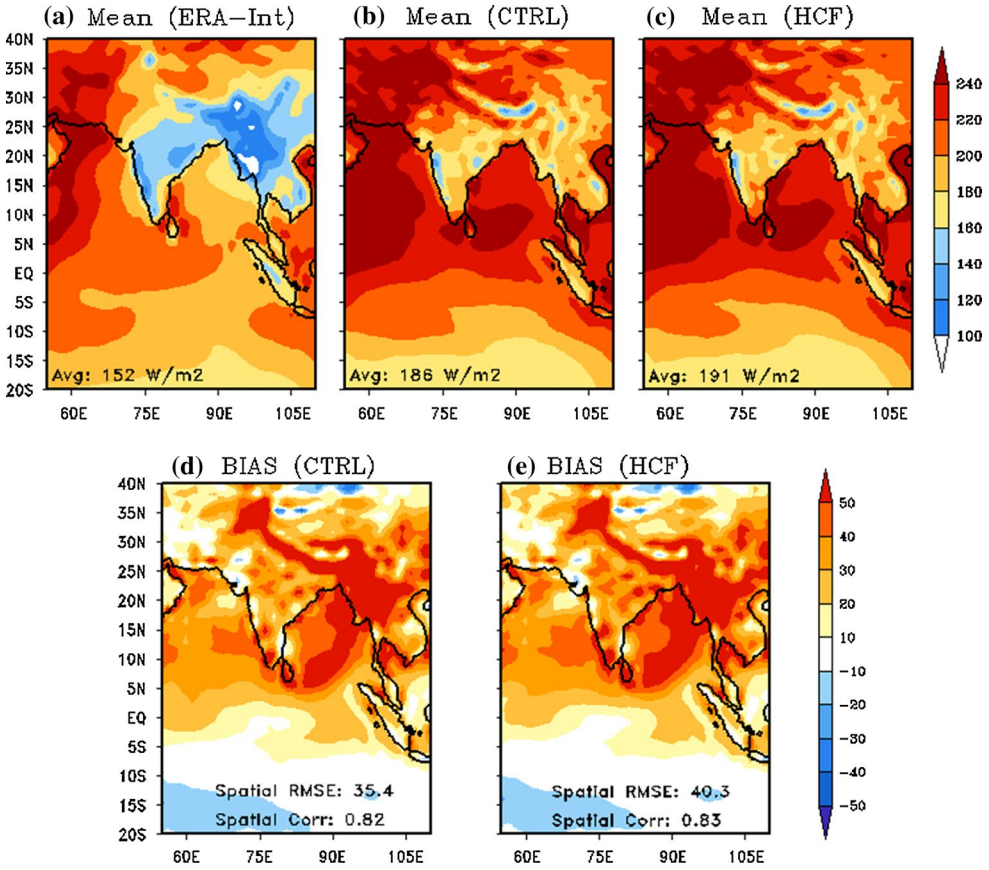

Fig. 9 Mean JJAS net surface shortwave radiation (W/m^2) for **a** ERA-interim, **b** CTRL, and **c** HCF and net shortwave bias for **d** CTRL and **e** HCF. The biases were calculated in relation to the ERA-interim reanalysis. The figure also shows information about net shortwave radiation average, spatial RMSE, and spatial correlation (in relation to ERA-interim) for the central India region

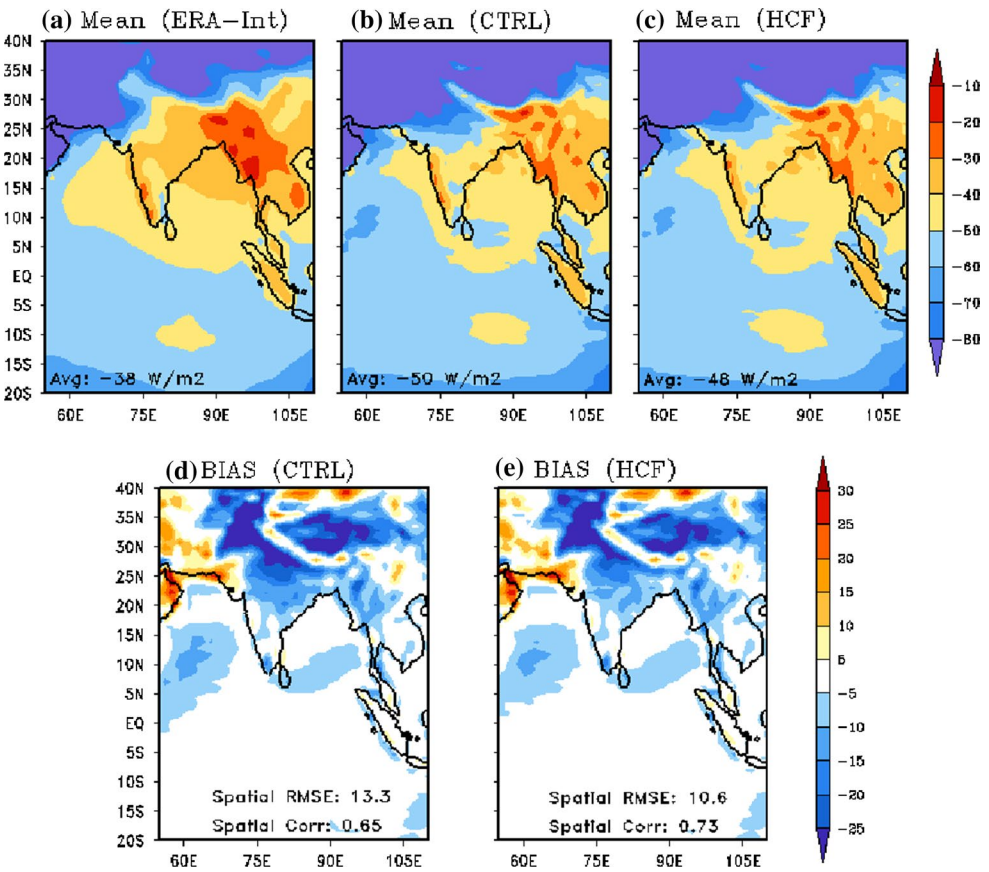

Fig. 10 As Fig. 9 for net surface longwave radiation

Author's personal copy

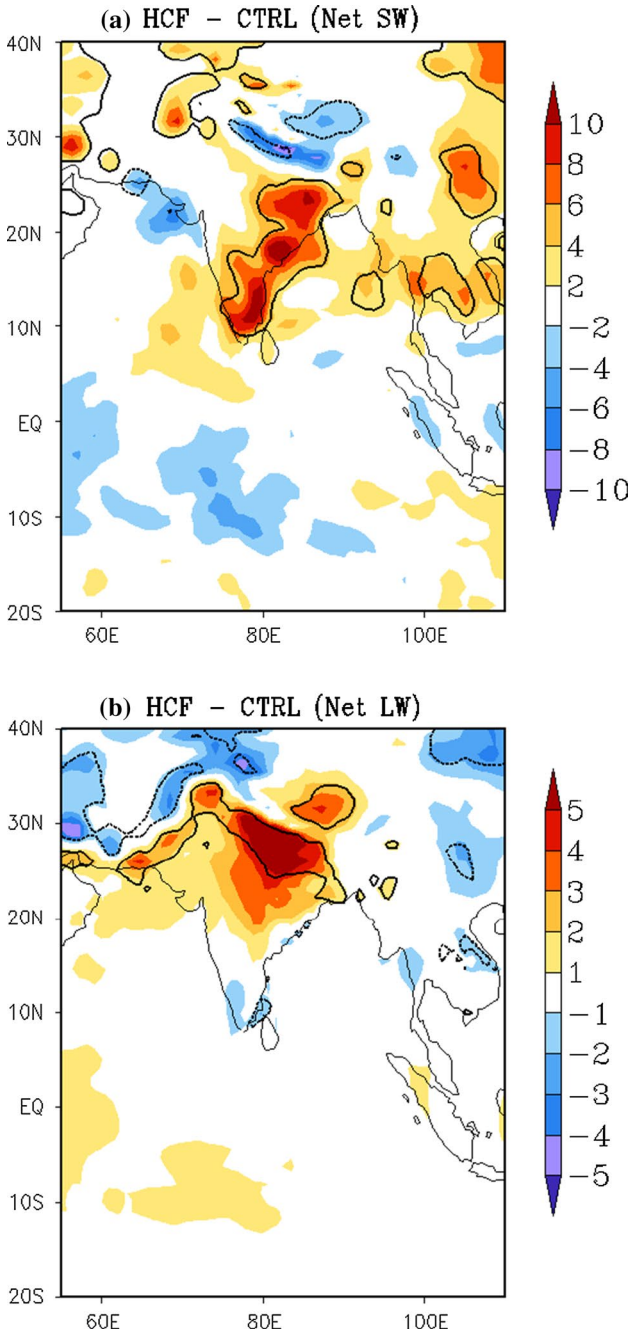

Fig. 11 Mean JJAS difference between HCF and CTRL for **a** net surface shortwave radiation and **b** net surface longwave radiation (W/m^2). The contour shows regions where the difference is statistically significant at 5 % level according to a *t* test

observed in the remaining regions (Fig. 12d, f, h). These results are consistent with the increase of short wave radiation (reduction of middle clouds) and increase of net surface longwave radiation (increase of high clouds) (Fig. 11). These results are also consistent with increased convective activity, where the cloud water is removed from the middle troposphere due to rainfall and injected into higher levels of the atmosphere driven by increased mixing and vertical motion (not shown).

As mentioned before, the HCF trigger needs two main conditions to trigger convection: A sufficiently moist atmosphere (quantified by θ_{BM}) and sufficient instability coming from surface heating (quantified by θ_{2m}). The lower the θ_{BM} the more is the atmosphere preconditioned for moist convection. To evaluate the difference in convective activity between HCF and CTRL we analyzed the simulated CAPE, which is one of the output variables in CFSv2, as well as θ_{2m} and θ_{BM}, which are important diagnostic variables for the HCF. We verify an increase in mean CAPE in HCF simulations in comparison to CTRL simulations over central–northeastern India (Fig. 13a). These results indicate that there is more intense convective instability in the HCF simulations than in the CTRL simulations. In addition, there is a reduction of θ_{2m} in the HCF simulations over central India in comparison to CTRL (Fig. 13b). This result is consistent with the development of a stronger monsoon system in the HCF simulations. Moreover, The HCF experiment showed colder θ_{BM} over central India than the CTRL experiment (Fig. 13c), indicating that convection was more likely to occur in the HCF experiment. Therefore, the significant changes in precipitation verified in the HCF simulations are associated with an increase in moist convective instability.

Although convective initiation does not directly influence the nature or the intensity of convection, over the long-term, the frequency of triggering convection modifies the accumulation of CAPE thereby impacting the intensity of convection and indirectly influencing the environment that is used by the SAS scheme.

It is relevant to point out that the convective triggering functions used in most models overlook the fact that the onset of cumulus convection in a grid column is a catastrophe (Chao 2013). A catastrophe is a rapid transition of a dynamical system from one (quasi) equilibrium to another. Therefore, once the criteria for convection initiation are met, the system continues in a convective state until the criteria for inhibition of convection are satisfied, regardless of whether or not the initiation criteria are still valid. As a result of overlooking the catastrophe concept, convection parameterizations over flat land tend to underestimate the amplitude of the diurnal cycle of precipitation and tend to simulate the peak of the diurnal cycle of precipitation too soon (Chao 2013). Chao (2013) designed a new method where the catastrophe concept is taken into consideration. The author implemented this new method into the Relaxed Arakawa–Schubert convection scheme (Moorthi and Suarez 1992) in the NASA's Goddard Earth Observing System GCM, version 5 (GEOS-5) and verified an improvement in the phase and amplitude of the precipitation diurnal cycle over relatively flat land.

Author's personal copy

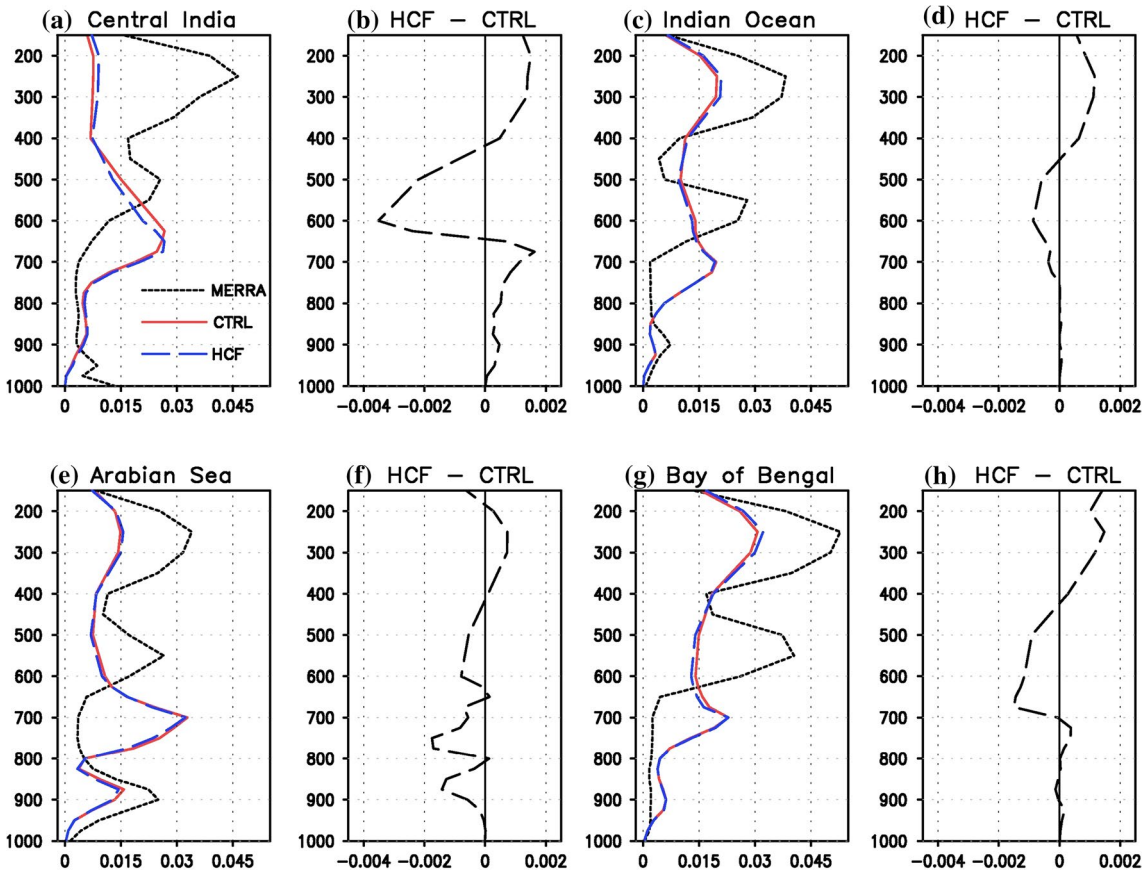

Fig. 12 Mean JJAS profiles of total cloud condensate (g/kg) for MERRA, CTRL, and HCF (**a**, **c**, **e** and **g**) and total cloud condensate difference between HCF and CTRL (**b**, **d**, **f**, and **h**). Spatially averaged over Central India (74.5°E–86.5°E, 16.5°N–26.5°N), the equatorial Indian Ocean (68°E–90°E, 5°S–5°N), the Arabian Sea (68°E–74°E, 10°N–22°N), and the Bay of Bengal (86°E–94°E, 14°N–22°N)

7 Conclusions

We present the sensitivity of the representation of the Indian summer monsoon resulting from the implementation of the HCF triggering mechanism for deep convection (Tawfik and Dirmeyer 2014) into the CFSv2. The HCF convective trigger mechanism is implemented as an alternative condition for deep convection to occur. The HCF trigger requires two main conditions to trigger convection: sufficient instability from surface heating and a sufficiently moist atmosphere.

The new trigger improves the representation of the Indian summer monsoon over central and northeastern India, reducing the CFSv2 precipitation bias and improving the simulation of seasonal and daily precipitation. Over central India, there is a clear improvement of the distribution of daily precipitation as well as in the annual cycle of precipitation. The HCF also improves the seasonal variability of precipitation over central and northeastern India as well as over the western coast of India, the Bay of Bengal, and the equatorial Indian Ocean. In addition, we verify an improvement in the monsoon timing over the entire Indian subcontinent and the probability distribution of precipitation intensity. However, only small differences were verified in the diurnal cycle of precipitation.

A better representation of deep convection is associated with a decrease of middle level clouds and an increase of high clouds over India. As a consequence, we verify an increase in net surface radiation, resulting in more energy at the surface in the HCF in comparison to the CTRL experiments. In addition, we verify an increase in convective activity in the HCF in comparison to the CTRL simulations.

The mechanism whereby the HCF trigger improves the representation of deep convection depends on several factors such as availability of moisture, atmospheric stability, and regional biases in the model. Therefore, there is a combination of factors that need to be taken into account when attributing precipitation changes to the HCF trigger. Specifically over India, the mechanism seems to be related to two main changes: (1) a better representation of the background state of convection and (2) an increase in the frequency in deep convection was initiated.

Author's personal copy

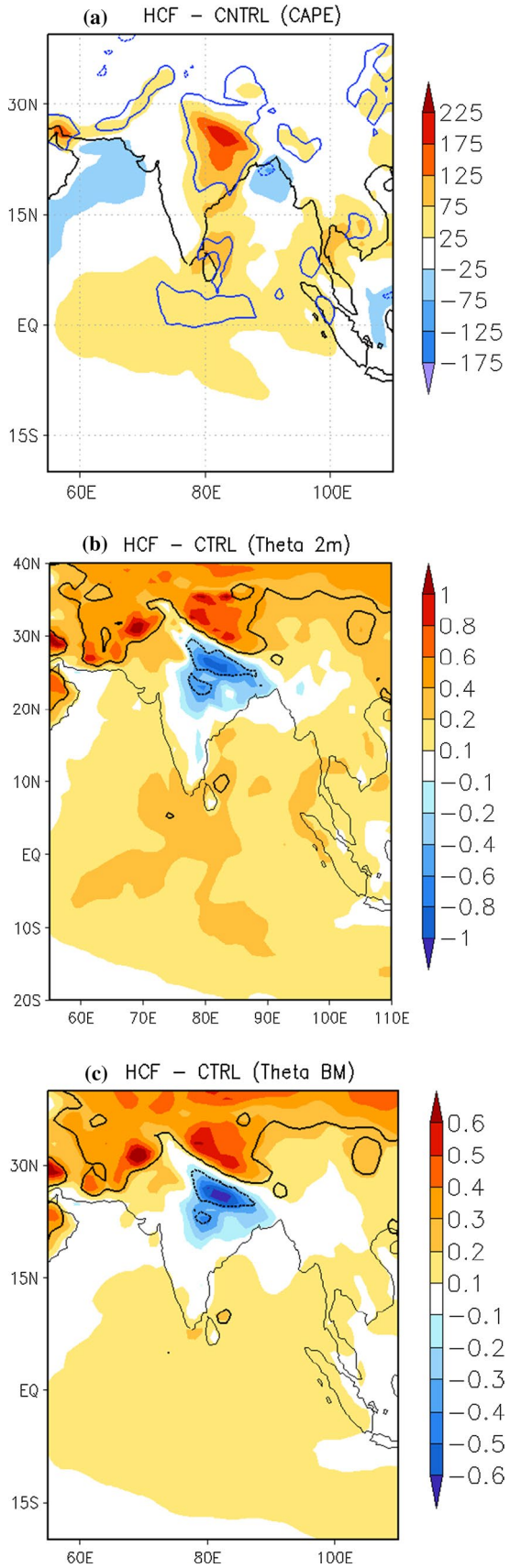

◀ **Fig. 13** **a** Mean JJAS CAPE (J/kg) difference between HCF and CTRL; **b** mean JJAS θ_{2m} (K) difference between HCF and CTRL and **c** mean JJAS θ_{BM} (K) difference between HCF and CTRL. Contour indicates regions where the difference is statistically significant at 5 % level according to a *t* test

Suhas and Zhang (2014) found that trigger functions show better skill when both instability and moisture are taking into consideration in their formulation. The authors verified that the Arakawa–Schubert trigger function could be optimized by the incorporation of a relative humidity threshold. Although we did not include a humidity threshold in the SAS scheme, the implementation of the HCF is a similar approach considering that the HCF criterion is the occurrence of condensation. Therefore, by implementing the HCF trigger, we included a combination of instability based and moisture based trigger functions into the SAS scheme, and the background state of convection could be better represented.

In addition, as we added the HCF criterion as an alternative condition for the initiation of deep convection, the convective scheme was triggered more often, allowing the system to produce more precipitation over India in comparison to CTRL. As a consequence, we verified a reduction of light precipitation and an increase of intense precipitation over central India, resulting in a simulated precipitation distribution that is closer to the precipitation distribution from observations. One may argue that the increase in the frequency of the activation of SAS could have increased precipitation anywhere. However, due to the conservation of total precipitation, precipitation cannot be increased everywhere and some regions will be more susceptible to changes than others. In the case of India, the increase in convective precipitation was favored by the availability of moist convective instability.

Therefore, the HCF triggering mechanism not only provides conditions that are more appropriated for tropical convection, it also improves the representation of the Indian summer monsoon by increasing precipitation intensity due to an increase in the frequency in which the convective scheme is activated, as long as convective instability conditions are met.

It is relevant to point out that the original triggering criterion is based on the lifting condensation level (LCL) and the HCF criterion is based on the BCL. Therefore, in some cases the LCL level can be fairly different from the BCL and, as a consequence, the level of the base of the convective cloud in the conceptual scheme. At this point, the HCF trigger is implemented solely as an indication for whether or not condensation occurs, regardless of whether or not LCL and BCL coincide. The SAS routine still uses the LCL as the cloud base level. We are currently investigating strategies to better integrate the HCF trigger into the SAS scheme in order to eliminate this inconsistency.

Author's personal copy

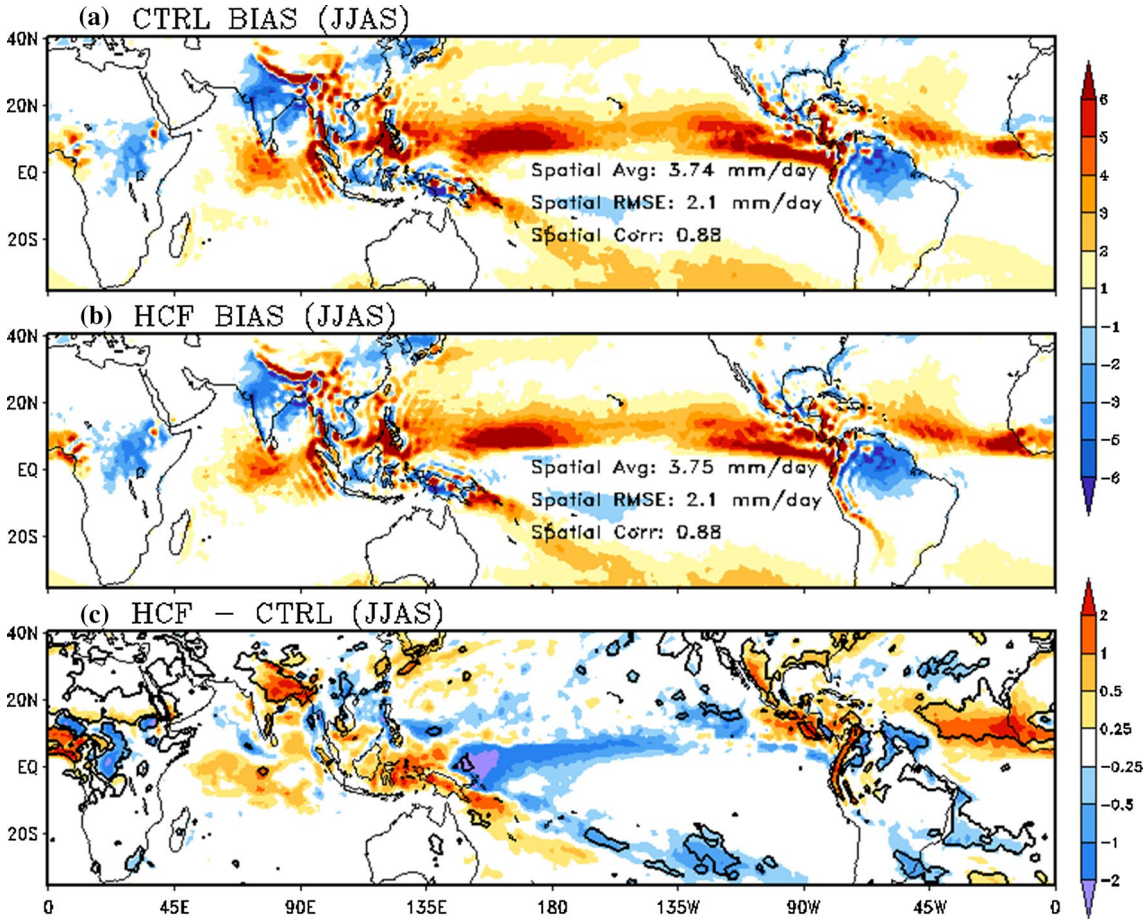

Fig. 14 Global JJAS precipitation (mm/day) bias for **a** CTRL and **b** HCF and **c** mean JJAS precipitation difference between HCF and CTRL. Contour indicates regions where the difference is statistically significant at 5 % level according to a *t* test. The figure also shows information about precipitation average, spatial RMSE, and spatial correlation (in relation to TRMM) for the entire domain

Since the CFSv2 still shows a large dry precipitation bias for the summer precipitation over India and a large wet bias over the ocean, further investigation is necessary. We are currently investigating strategies to further improve the CFSv2 representation of convective precipitation. These strategies include the tuning of the HCF trigger, the reduction of the model time step, and the improvement of the HCF trigger. A new version of the HCF trigger with a better representation of convection initiation over the ocean is currently in test for this purpose.

Acknowledgments We thank the support from the National Monsoon Mission, Ministry of Earth Sciences, Government of India. We also thank the support from NSF (0830068), NOAA (NA09OAR4310058) and NASA (NNX09AN50G). We thank the two anonymous reviewers for their suggestions for the improvement of this manuscript. In addition, we thank the European Centre for Medium-Range Weather Forecasts (ECMWF) for making available the ERA-interim reanalysis and the National Aeronautics and Space Administration (NASA) for making available the MERRA reanalysis and the TRMM analysis. This work used the Extreme Science and Engineering Discovery Environment (XSEDE), which is supported by National Science Foundation grant number ACI-1053575.

Appendix: Precipitation changes in the tropics

Figure 14 shows the JJAS precipitation bias for the entire tropics as well as the difference between HCF and CTRL. As mentioned before, the new triggering mechanism causes only small changes in the CFSv2 precipitation bias (Fig. 14a, b). Besides changes in the Indian summer monsoon, there are significant differences in precipitation over the Central America, the Amazon, tropical Atlantic Ocean, and tropical Africa (Fig. 14c). Although the new trigger improves precipitation over the Indian region, the magnitude of the bias increases over the tropical Atlantic and over tropical Africa (Fig. 14c). Consistent results (slightly smaller differences) are observed when evaluating the simulations for different periods, such as May through July

Author's personal copy

(not shown). This is an example of a well-known phenomenon in developing climate models. When making model modifications it is common to observe the improvement of some regions and the detriment of others. The most important aspect of this research is the fact that we are making the parameterization more physically realistic. In addition, biases can be compensated in the future from the other parameterizations that were tuned to have the best performance in relation to the prior convective trigger.

Presumably, the changes in the precipitation biases in the Indian region could be due to changes in convection elsewhere, like the tropical Pacific, due to teleconnections. However, we did not identify significant circulation changes showing wave-like patterns between HCF and CTRL simulations (not shown). Rather, the changes in circulations are very local. Therefore, although remote influences could be playing a role in the changes in the precipitation biases over India, the mechanisms discussed in the conclusions are likely the dominant mechanisms.

References

Bombardi RJ, Carvalho LMV (2009) IPCC global coupled model simulations of the South America monsoon system. Clim Dyn 33:893–916. doi:10.1007/s00382-008-0488-1

Chao WC (2012) Correction of excessive precipitation over steep and high mountains in a GCM. J Atmos Sci 69:1547–1561. doi:10.1175/JAS-D-11-0216.1

Chao WC (2013) Catastrophe-concept-based cumulus parameterization: correction of systematic errors in the precipitation diurnal cycle over land in a GCM. J Atmos Sci 70:3599–3614. doi:10.1175/JAS-D-13-022.1

Dee DP, Uppala SM, Simmons AJ et al (2011) The ERA-interim reanalysis: configuration and performance of the data assimilation system. Q J R Meteorol Soc 137:553–597. doi:10.1002/qj.828

Fasullo J, Webster PJ (2002) Hydrological signatures relating the Asian summer monsoon and ENSO. J Clim 15:3082–3095. doi:10.1175/1520-0442(2002)015<3082:HSRTAS>2.0.CO;2

Griffies SM, Harrison MJ, Pacanowski RC, Rosati A (2004) A technical guide to MOM4. GFDL ocean group technical report no. 5. 281

Han J, Pan H-L (2011) Revision of convection and vertical diffusion schemes in the NCEP global forecast system. Weather Forecast 26:520–533. doi:10.1175/WAF-D-10-05038.1

Hong S-Y, Pan H-L (1998) Convective trigger function for a mass-flux cumulus parameterization scheme. Mon Weather Rev 126:2599–2620

Huffman GJ, Bolvin DT, Nelkin EJ et al (2007) The TRMM multisatellite precipitation analysis (TMPA): quasi-global, multiyear, combined-sensor precipitation estimates at Fine Scales. J Hydrometeorol 8:38–55. doi:10.1175/JHM560.1

Joseph PV, Eischeid JK, Pyle RJ (1994) Interannual variability of the onset of the Indian summer monsoon and its association with atmospheric features, El Niño, and sea surface temperature anomalies. J Clim 7:81–105. doi:10.1175/1520-0442(1994)007<0081:IVOTOO>2.0.CO;2

Kang I-S, Yang Y-M, Tao W-K (2014) GCMs with implicit and explicit representation of cloud microphysics for simulation of extreme precipitation frequency. Clim Dyn. doi:10.1007/s00382-014-2376-1

Kumar S, Hazra A, Goswami BN (2013) Role of interaction between dynamics, thermodynamics and cloud microphysics on summer monsoon precipitating clouds over the Myanmar Coast and the Western Ghats. Clim Dyn 43:911–924. doi:10.1007/s00382-013-1909-3

Liebmann B, Marengo JA (2001) Interannual variability of the rainy season and rainfall in the Brazilian Amazon Basin. J Clim 14:4308–4318. doi:10.1175/1520-0442(2001)014<4308:IVOTRS>2.0.CO;2

Moorthi S, Suarez MJ (1992) Relaxed Arakawa–Schubert. A parameterization of moist convection for general circulation models. Mon Weather Rev 120:978–1002. doi:10.1175/1520-0493(1992)120<0978:RASAPO>2.0.CO;2

Pan H-L, Wu W-S (1995) Implementing a mass flux convective parameterization package for the NMC medium range forecast model. NMC Off Note 409. http://www.emc.ncep.no

Pokhrel S, Chaudhari HS, Saha SK et al (2012) ENSO, IOD and Indian summer monsoon in NCEP climate forecast system. Clim Dyn 39:2143–2165. doi:10.1007/s00382-012-1349-5

Rienecker MM, Suarez MJ, Todling R, et al. (2008) The GEOS-5 data as- similation system—documentation of versions 5.0.1 and 5.1.0, and 5.2.0. NASA Tech. Rep. Series on global modeling and data assimilation, NASA/TM-2008-104606/Vol 27

Rienecker MM, Suarez MJ, Gelaro R et al (2011) MERRA: NASA's modern-era retrospective analysis for research and applications. J Clim 24:3624–3648. doi:10.1175/JCLI-D-11-00015.1

Rienecker MM, Dee D, Woollen J, et al. (2012) Atmospheric reanalyses—recent progress and prospects for the future. NASA Tech. Rep. Series on Global Modeling and Data Assimilation, NASA/TM–2012-104606/Vol 29

Saha S, Nadiga S, Thiaw C et al (2006) The NCEP climate forecast system. J Clim 19:3483–3517. doi:10.1175/JCLI3812.1

Saha S, Moorthi S, Pan H-L et al (2010) The NCEP climate forecast system reanalysis. Bull Am Meteorol Soc 91:1015–1057. doi:10.1175/2010BAMS3001.1

Saha S, Moorthi S, Wu X et al (2014a) The NCEP climate forecast system version 2. J Clim. doi:10.1175/JCLI-D-12-00823.1

Saha SK, Pokhrel S, Chaudhari HS et al (2014b) Improved simulation of Indian summer monsoon in latest NCEP climate forecast system free run. Int J Climatol 34:1628–1641. doi:10.1002/joc.3791

Silva GAM, Dutra LMM, da Rocha RP et al (2014) Preliminary analysis on the global features of the NCEP CFSv2 seasonal hindcasts. Adv Meteorol 2014:1–21. doi:10.1155/2014/695067

Smith RB, Minder JR, Nugent AD et al (2012) Orographic precipitation in the tropics: the Dominica experiment. Bull Am Meteorol Soc 93:1567–1579. doi:10.1175/BAMS-D-11-00194.1

Stevens B (2005) Atmospheric moist convection. Annu Rev Earth Planet Sci 33:605–643. doi:10.1146/annurev.earth.33.092203.122658

Suhas E, Zhang GJ (2014) Evaluation of trigger functions for convective parameterization schemes using observations. J Clim. doi:10.1175/JCLI-D-13-00718.1

Tawfik AB, Dirmeyer PA (2014) A process-based framework for quantifying the atmospheric preconditioning of surface-triggered convection. Geophys Res Lett 41:173–178. doi:10.1002/2013GL057984

Yang S, Zhang Z, Kousky VE et al (2008) Simulations and seasonal prediction of the Asian summer monsoon in the NCEP climate forecast system. J Clim 21:3755–3775. doi:10.1175/2008JCLI1961.1

Zhu J, Shukla J (2013) The role of air–sea coupling in seasonal prediction of Asia–Pacific summer monsoon rainfall. J Clim 26:5689–5697. doi:10.1175/JCLI-D-13-00190.1